

Article

Kinetics of Bainite Transformation in Multiphase High Carbon Low-Silicon Steel with and without Pre-Existing Martensite

Zeinab Babasafari ^{1,*}, Alexey V. Pan ², Farshid Pahlevani ³, Suk Chun Moon ⁴, Madeleine Du Toit ⁴ and Rian Dippenaar ⁴

¹ Division of Research and Enterprise, University of New South Wales (UNSW Sydney), Sydney, NSW 2052, Australia

² Institute for Superconducting and Electronic Materials, University of Wollongong, Wollongong, NSW 2522, Australia

³ Centre for Sustainable Materials Research and Technology (SMaRT Centre), School of Materials Science and Engineering, University of New South Wales (UNSW Sydney), Sydney, NSW 2052, Australia

⁴ School of Mechanical, Materials, Mechatronic and Biomedical Engineering, University of Wollongong, Wollongong, NSW 2522, Australia

* Correspondence: z.babasafari@unsw.edu.au

Abstract: In the present study, the isothermal decomposition of austenite to bainite in 1.0 wt% carbon, 0.21% silicon steel during the partitioning step of a quenching and partitioning (Q&P) heat treatment has been investigated in a dilatometer in the temperature range of 200 to 350 °C and compared to conventional austempering heat treatment. The bainite transformation was shortened by about 75% in the presence of pre-existing martensite (QP). The kinetics of bainite transformation is described by the well-known Avrami equation. The calculated parameter ‘n’ in the Avrami equation shows that bainite forms in the absence of pre-existing martensite (TT) at a constant nucleate rate, while in the presence of pre-existing martensite, nucleation is interface controlled. The overall bainite transformation activation energy, calculated by the Avrami equation, ranges from 64 to 110 kJ/mol. The outcomes of this investigation provide guidelines for the development of multiphase microstructures, including pre-existing martensite and bainite in high-carbon low-silicon steel, within an industrially acceptable time scale and mechanical performance.

Keywords: high-carbon steel; bainite; Q&P; pre-existing martensite; activation energy; Avrami equation



Citation: Babasafari, Z.; Pan, A.V.; Pahlevani, F.; Moon, S.C.; Du Toit, M.; Dippenaar, R. Kinetics of Bainite Transformation in Multiphase High Carbon Low-Silicon Steel with and without Pre-Existing Martensite. *Metals* **2022**, *12*, 1969. <https://doi.org/10.3390/met12111969>

Academic Editor: Zhinan Yang

Received: 14 October 2022

Accepted: 16 November 2022

Published: 18 November 2022

Publisher's Note: MDPI stays neutral with regard to jurisdictional claims in published maps and institutional affiliations.



Copyright: © 2022 by the authors. Licensee MDPI, Basel, Switzerland. This article is an open access article distributed under the terms and conditions of the Creative Commons Attribution (CC BY) license (<https://creativecommons.org/licenses/by/4.0/>).

1. Introduction

Quenching and partitioning (Q&P) heat treatments have been extensively applied to low-carbon steels in order to provide multiphase microstructures that provide a suitable combination of strength and ductility [1–5]. By this process, a mixture of martensite and retained austenite (RA) is attained by carbon diffusion from supersaturated martensite to untransformed austenite during the isothermal partitioning step [6,7]. The isothermal decomposition of austenite to bainite during the partitioning step is normally not considered, yet it plays an important role in determining the mechanical properties of the steel [8] and yet, only a few studies have considered the development of multiphase microstructure-containing bainite [9]. It seems possible that there is competition of bainite formation from retained austenite and carbon partitioning in high-carbon steel with a low silicon content (<1.5%) [10–14].

A lower-bainite microstructure in high-carbon steel provides an excellent combination of strength and toughness for industrial applications, specifically for the manufacturing of wear-resistant components. Hardness in excess of 650 HV can be achieved by the isothermal transformation of austenite to bainite at low temperatures [15]. Such lower-bainite structures have lower crack growth rates than tempered martensite [16], but the main challenge for developing nanoscale bainitic microstructures is to design a suitable

steel composition and heat-treatment parameters so that complete transformation can be achieved within an industrially acceptable time scale [11,15,17,18].

It is well known that pre-existing martensite strongly affects the kinetics of bainite transformation in low-carbon steel [19–21]. Santofimia et al. have shown that in low-carbon steel, the bainitic transformation is accelerated by the presence of pre-existing martensite [19,20,22,23]. By contrast, Smanio examined the effects of 15% and 30% pre-existing martensite in 100Cr6 steel, a commercial grade high-carbon bearing steel, at tempering/partitioning temperatures of 220 and 250 °C and found that the bainite transformation kinetics was not influenced by the presence of pre-existing martensite [24]. Vettters argued that pre-existing martensite not only accelerates bainite transformation kinetics at a temperature of 230 °C in the same steel type, but it also enhances fatigue resistance, while the hardness remains constant [25]. Toji et al. observed the acceleration of bainite transformation in high-carbon silicon-free steel at a transformation temperature of 300 °C. They suggest that dislocations introduced by prior martensite accelerate bainite nucleation [26]. Hu et al. compared low-temperature bainite transformation with a quenching–partitioning–tempering heat treatment in a high-carbon steel containing C 0.95%, Si 0.91%, Mn 1.3%, and Cr 2.3% and showed that nanoscale microstructures consisting of martensite, retained austenite, and fine carbides produced by a two-step heat treatment is harder than a low-temperature bainite microstructure produced by isothermal transformation at 200 °C for 240 h [27].

Many efforts have been expended in attempts to better understand and to develop kinetic models in order to predict carbon partitioning and bainite formation, but it seems that there is not an agreed-upon method as yet [23,28–30]. The Johnson–Mehl–Kolmogorov–Avrami equation (JMKA), for the sake of simplicity referred as the Avrami model, is currently the most acceptable equation to model the isothermal transformation of austenite to bainite [31–35].

In the present study, the kinetics of the bainite transformation with and without pre-existing martensite was analyzed by the use of the Avrami equation in the temperature range 200 to 350 °C and the overall activation energy was calculated by the Arrhenius equation. These results provide guidelines to develop multiphase microstructures with suitable mechanical properties for industrial applications of high-carbon low-silicon steel.

2. Materials and Methods

Industrially produced forged steel balls 1 wt% C, 0.98 wt% Mn, 0.18 wt% Cu, 0.63 wt% Cr, and 0.21 wt% Si alloy were used in the present study. In order to compare the kinetics of the austenite-to-bainite transformation in the presence and absence of pre-existing martensite (QP versus TT), isothermal temperatures of 200, 250, 300, and 350 °C were selected.

The isothermal decomposition of austenite to bainite in the temperature range 200–350 °C was investigated using a Theta Dilatronic III and compared with the partitioning step of a quenching and partitioning (Q&P) heat treatment in the similar temperature range, as shown in Figure 1. The martensite start temperature was determined as 151 °C by dilatometry prior to the design of the two-step heat treatments. In Q&P heat treatments, specimens were fully austenized at 1000 °C for 30 min and quenched with helium gas to 100 °C within the dilatometer, and then held for 10 s to generate martensite and retained austenite. The specimens were then heated to temperatures between 200 and 350 °C before a secondary quench to room temperature was applied. The holding time was extended for both one-step and two-step heat treatments until a steady-state condition was achieved (where the bainitic transformation ratio would be 100% in the dilatometry analysis). The dilatometry data were used to calculate the transformation rates, which were used to characterize the bainite reaction kinetics following isothermal heat treatment and also to calculate the activation energy [36].

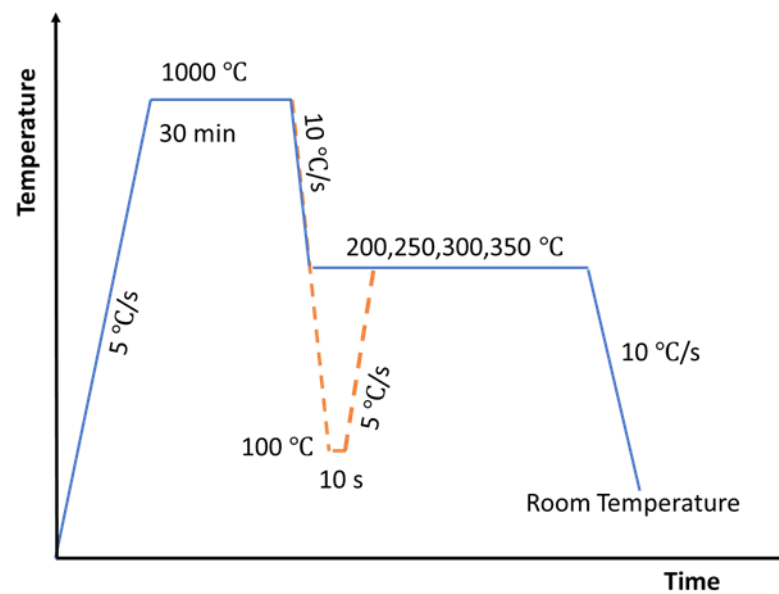


Figure 1. Schematic view of the different heat treatment schedules (temperature vs. time) used in this work.

The fraction of retained austenite (RA) was quantified using a Quantum Design MPMS SQUID magnetometer, while the martensite and bainite phase fractions were respectively calculated from the dilatometry analysis. Micro Vickers hardness measurements were made by the use of Matsuzawa Via-F automatic Vickers hardness testing. A load of 1 kg was used and a minimum of five measurements were made on a given sample. The experimental methods and microstructural features have been described in detail in previously published research [37–39].

3. Results and Discussion

3.1. Role of Pre-Existing Martensite on Bainite Formation

Pre-existing martensite accelerates bainite formation in low-carbon steel, but this does not seem to be the case in high-carbon steel. In an attempt to resolve these apparent discrepancies outlined in the introduction above, the two-step heat treatment, illustrated in Figure 1, was implemented. However, the holding time was extended to a point where a steady-state condition was obtained and where no more austenite transformed to bainite. In these isothermal heat treatments, the samples were austenitized at 1000 °C and then quenched directly to a temperature in the range of 200 to 350 °C and held isothermally until the austenite fully transformed to bainite before they were quenched to room temperature (Bf). The holding time was extended until all of the austenite transformed into bainite at all of the isothermal temperatures except for a temperature of 200 °C, where the transformation of retained austenite to bainite was not completed, even after 24 h (TT200). The relative change in length ($\Delta L/L_0$) versus the holding time at the chosen isothermal steps is shown in Figure 2. In the legend QPX-Y, TTX-Y, X indicates the isothermal holding temperature in degrees centigrade (°C) while Y indicates the holding time in hours (hr.) or minutes (min).

Two different sets of experiments were conducted: isothermal heat treatments by quenching directly to the isothermal transformation temperature as outlined above, and another set by firstly introducing a small percentage of pre-existing martensite. The small fraction of pre-existing martensite was introduced by quenching to 100 °C (51 °C below the martensite start temperature), as shown in Figure 1. The bainite start and finishing times were determined from the dilatometry curves prior to calculating the bainite transformation time, as shown in Table 1. In this table, Bs-TT and Bf-TT indicate bainite starting and finishing times, respectively, in the absence of pre-existing martensite, while Bs-QP and Bf-QP show the corresponding starting and finishing times in the presence of pre-existing martensite. Table 1 shows that the starting time for bainite formation, (Bs), decreased

sharply and the austenite transformation to bainite finished quicker in the presence of pre-existing martensite.

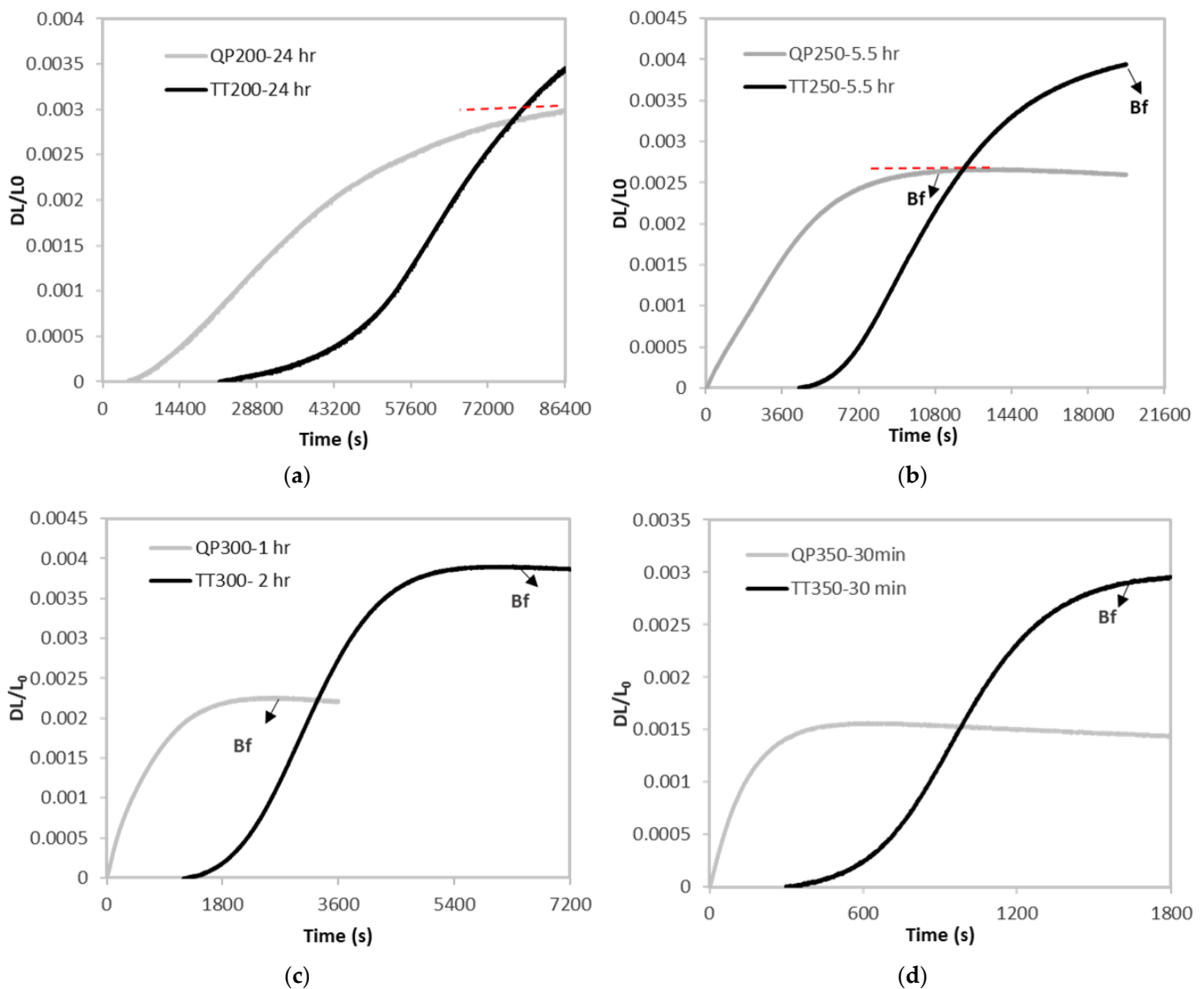


Figure 2. Dilatation during bainitic formation in one-step (TT) and two-step (QP) heat treatments: (a) 200 °C; (b) 250 °C; (c) 300 °C; (d) 350 °C.

Table 1. Bainitic transformation start and finishing times for different heat treatments.

Holding Temperature (°C)	Bs-TT (s)	Bf-TT (s)	Bs-QP (s)	Bf-QP (s)	Transformation Reduction Time (%)
200	21,800	>86,400	4800	86,400	-
250	4400	19,800	45	11,800	40
300	1120	5350	0	2000	63
350	300	1800	0	540	70

These experimental measurements are interesting because they are in conflict with the earlier findings of Veronique et al., who found that pre-existing martensite did not affect bainite formation at such at low temperatures [27].

Figure 2c,d shows that the transformation of austenite to bainite starts instantly at temperatures of 300 and 350 °C in the presence of pre-existing martensite (QP-300 and QP-350).

At 200 °C, bainite formation starts earlier in the presence of pre-existing martensite (4800 s versus 21,800 s) and the transformation is completed within 24 h (Figure 2a). Bainite starts to form at 250 °C after 90 min in the absence of pre-existing martensite, while it starts to transform within 45 s in the presence of pre-existing martensite (Figure 2b). The time taken to form a fully bainitic structure is shortened by 70% and 63% at isothermal transformation temperatures of 350 and 300 °C, respectively. The effect of pre-existing martensite on the acceleration of bainite formation is smaller at lower temperatures; specifically, the bainitic formation time is reduced by only 40% at a transformation temperature of 250 °C. By calculating the dilatation at any holding time divided by the maximum dilatation, the so-called ‘bainite formation ratio’ is calculated as shown in Figure 3. This ratio provides clear evidence that pre-existing martensite has a significant effect on the starting of bainite formation. Some SEM metallographic investigations have already been published in Figure 13 of reference [37], Figures 2 and 3 of reference [38] and Figure 7 of reference [39].

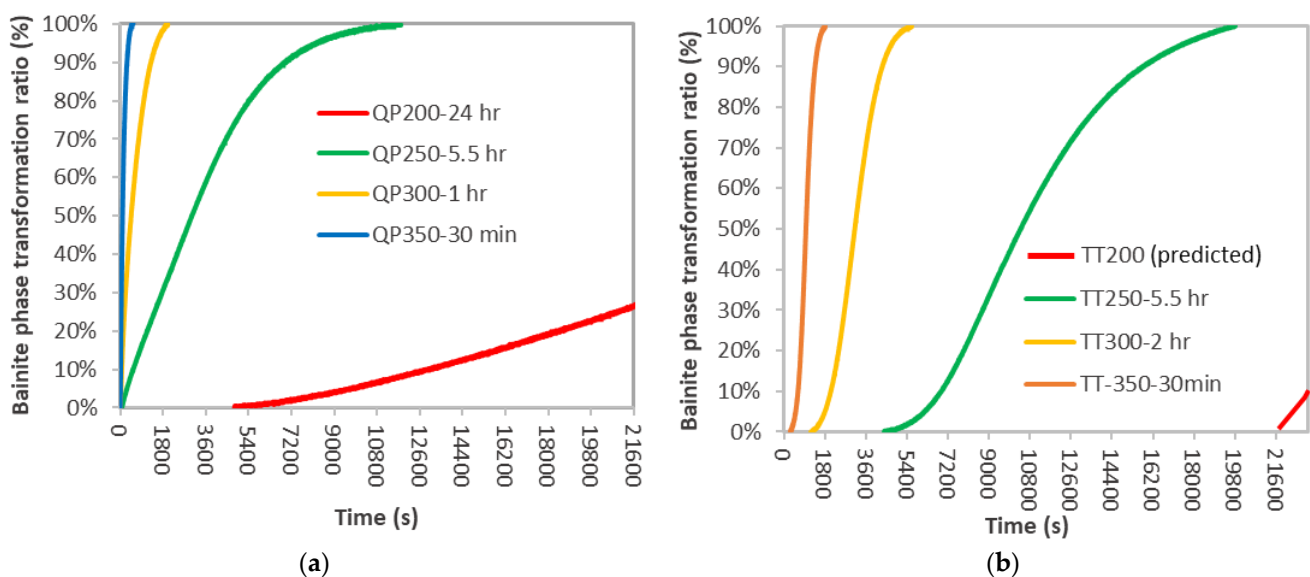


Figure 3. Bainite transformation ratio: (a) quenching partitioning; (b) isothermal.

3.2. Hardness Measurement and the Fraction of Retained Austenite

The hardness measurements made on the dilatometry samples with and without pre-existing martensite (TT and QP, respectively) are shown in Figure 4. The error bars represent the 95% confidence interval. The hardness increases by a decrease in the transformation temperature. The corresponding fractions of retained austenite are shown in Table 2.

The hardness of the austempered (TT) and quenching-and-partitioning samples (QP) at a temperature of 350 °C is similar (570 HV). Moreover, the retained austenite phase fractions were similar. The hardness of the austempered sample (TT200) at a temperature of 200 °C is higher than the corresponding QP200 sample (738.3 versus 714 HV), while the retained austenite phase fraction is much higher, 36.8% versus 20%. The hardness of TT200 is higher than that of QP200, presumably due to the presence of fresh martensite [37–39].

The hardness of samples heat treated in a two-step heat treatment (QP) at 250 and 300 °C are higher than the corresponding samples that were treated isothermally (TT), most likely because they contained less retained austenite and because of the presence of tempered martensite in the QP samples [37–39].

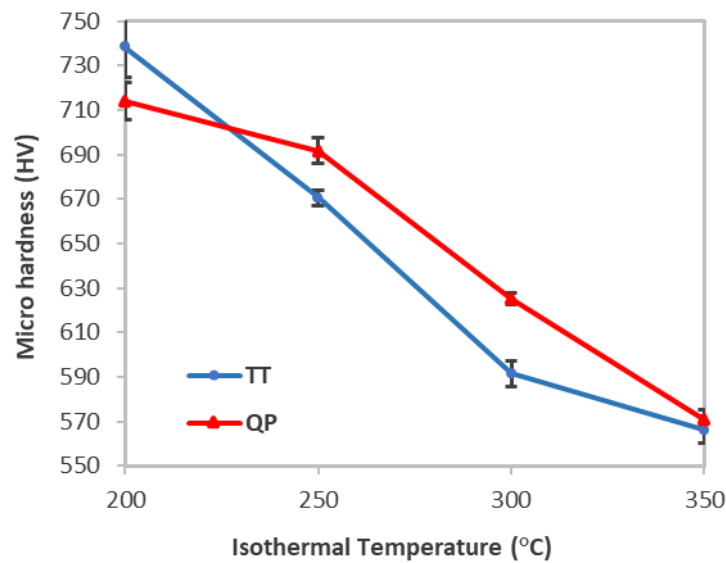


Figure 4. Hardness measurement at different tempering temperatures.

Table 2. RA phase fraction of TT and QP conditions.

Temperature (°C)	TT	QP
	RA%–Holding Time	RA%–Holding Time
200	36.8%–24 h	20.0%–24 h
250	9.2%–5.5 h	7.0%–5.5 h
300	10.0%–2 h	4.8%–1 h
350	4.0%–30 min	7.8%–30 min

3.3. Kinetics of Bainite Formation

The popular Johnson–Mehl–Kolmogorov–Avrami equation (JMKA), often used to model isothermal transformation kinetics, assumes that nucleation occurs randomly in untransformed austenite, while growth occurs at the same rate in all directions independent of the extent of transformation. The equation links time and the transformed phase volume fraction at a specific temperature as per Equation (1), where k and n are constants.

$$x(t) = 1 - \exp(-Kt^n) \quad (1)$$

where $x(t)$ is the fraction of the new phase (in this case, the bainite transformation ratio), t is transformation time. K determines the rate of transformation (1/s) in order to explore the nucleation and crystal growth processes. The parameter ‘ n ’ identifies the shape of the bainite/ferrite phase (needle, plate, sphere) and transformation mode (one-dimensional, grain boundary, volume growth). A value of ‘ n ’ in the range 1 to 4 has been reported in many studies [30–34,40].

By applying logarithms, a linear relationship is obtained between $\log(-\ln(1 - X))$ and $\log(t)$.

$$\log(-\ln(1 - x(t))) = n \times \log(t) + \log(K) \quad (2)$$

The values of K and n can be obtained from the linear regression adjustment of experimental data obtained by dilatometry by plotting $\log(-\ln(1 - x(t)))$ versus $\log(t)$ at a constant temperature. Figure 5 shows the linear fitting of the TT and QP heat treatments. The linear regression is shown by the dashed black lines. The measured values are shown in Table 3. The specific values of K and n depend on the nature of nucleation and growth [40,41]. In this table, R^2 indicates the R-squared value for a linear regression of a specific heat treatment. In Figure 5, TT refers to isothermal transformation without

pre-existing martensite, while QP indicates the presence of pre-existing martensite. In table QPX-Y, the Y indicates the holding time at any specific temperature (X).

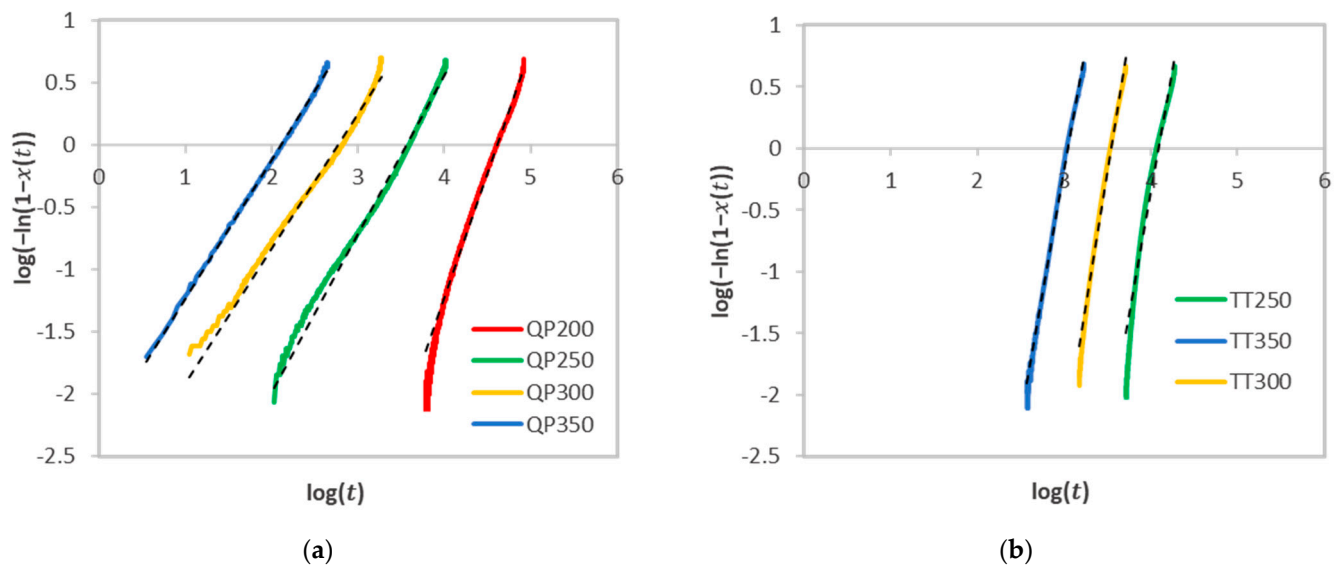


Figure 5. Linear fitting of $\log(-\ln(1-x(t)))$ and $\log(t)$: (a) QP (b) TT.

Table 3. Summary of the Avrami constants n and K for high-carbon steel.

Heat Treatment Condition	n	Log (K)	K	R^2
QP200–24 h	1.9959	−9.2155	6.088×10^{-10}	0.9925
QP250–5.5 h	1.2741	−4.5359	2.911×10^{-5}	0.9924
QP300–1 h	1.0813	−2.9928	1.017×10^{-3}	0.9872
QP350–30 min	1.1158	−2.3564	4.401×10^{-3}	0.9972
TT250–5.5 h	3.8976	−15.9480	1.127×10^{-16}	0.9620
TT300–2 h	4.1313	−15.2910	5.11×10^{-16}	0.9902
TT350–30 min	4.0090	−12.1970	6.35×10^{-13}	0.9949

In the isothermal transformation temperature range of 250 to 350 °C in the absence of pre-existing martensite, the value of n is approximately 4, which implies a constant nucleation rate and three-dimensional linear growth of bainite. This value of n is in agreement with an average value of $n = 4.5$ reported for a commercial grade of high-carbon steel 100Cr6 [40].

In the two-step heat treatment, the value of $n < 2$, which, according to the literature, implies that the transformation to bainite is nucleation controlled and that, at 200 °C, the morphology of growth is disk-like shaped and the growth is linear [41].

3.4. Activation Energy

The kinetics of the austenite to bainite transformation is determined by nucleation and growth kinetics as well as the morphology and is linked to the Gibbs free energy of transformation. The overall activation energy of the bainite transformation constitutes the driving force for this transformation. A simplified Arrhenius equation is usually applied to determine the activation energy of the phase transformation:

$$K = Ae^{-Q/RT} \quad (3)$$

where

K—rate of reaction (1/s),

Q—overall activation energy (J/mol),

T—temperature (K),
 R—gas constant 8.31 (J/mol·K),
 A—constant dependent on frequency (1/s).

The apparent activation energy of the overall bainite transformation takes into account the energy required to form bainite from grain-boundary nucleation sites, autocatalytic nucleation at the newly created ferrite/austenite interfaces or pre-existing martensite/austenite interfaces, subsequent carbon partitioning, and also the effect that dislocations may have [23,28,41,42]. In most cases reported in the literature, the activation energy ranges from 50 to 167 kJ/mol [36] and specifically reported as 50 kJ/mol for a commercially produced high-carbon steel 100Cr6 [40]. By applying logarithms, a linear relationship is found between $\ln(K)$ and $\frac{1}{T}$; the activation energy can then be calculated by Equation (4).

$$\ln K = \ln A - \frac{Q}{R} \cdot \frac{1}{T} \quad (4)$$

Many researchers have used 50% transformation as a measure of the rate [43]. In this study, 10%, 50%, and 90% transformation points have been chosen and compared in order to ensure the validity of the calculations. In this formula, K is ($K = 1/t_i$). The t_i is the chosen transformation time, which in this study is 10, 50, or 90%. These times were measured experimentally from the pertaining dilatometer curves (Figure 2). By replacing $K = 1/t_i$ in the Arrhenius equation and applying logarithmic in both sides of the equation:

$$\ln(t_i) = \frac{Q}{R} \cdot \frac{1}{T} - \ln(A) \quad (5)$$

The slope of the linear regression between $\ln(t_i)$ and $1/T$ is Q/R [44]. The data used to calculate the activation energy are shown in Table 4.

Table 4. Data used for calculating overall activation energy of bainite transformation in different transformation points.

Heat Treatment	Temperature (K)	t_{10} (s)	t_{50} (s)	t_{90} (s)
QP200–24 h	473	12,950	32,894	65,625
QP250–5.5 h	523	540	3007	6912
QP300–1 h	573	63	456	1278
QP350–30 min	623	16	94	280
Activation energy QP (kJ/mol)		110.0	99.6	88.7
TT250–5.5 h	523	6906	10381	15800
TT300–2h	573	2059	3110	4310
TT350–30 min	623	630	968	1366
Activation energy TT (kJ/mol)		64.7	64.2	66.3

Figure 6 shows the best linear fit for the different heat treatments.

The activation energy for the one-step isothermal transformation is about 65 kJ/mol regardless of the transformation ratios. It is very close to the reported activation energy for the diffusion of carbon in ferrite, 70 kJ/mol. By comparison, Vasudevan et al. reported the same value for the activation energy of lower bainite based on a transformation ratio of 50% in carbon steel containing 0.97 mass %C [41,43].

For Q&P heat treatments, the activation energy is higher than that for isothermal transformation in the absence of pre-existing martensite. This means that more energy is required for carbon diffusion into ferrite in the presence of pre-existing martensite. The value of the activation in this case lies between 110 and 88.7 kJ/mol. when the transformation ratio is increased from 10% to 90%.

These values of the activation energy seem to suggest that pre-existing martensite initially acts as nucleation sites for the transformation of the austenite surrounding the martensite.

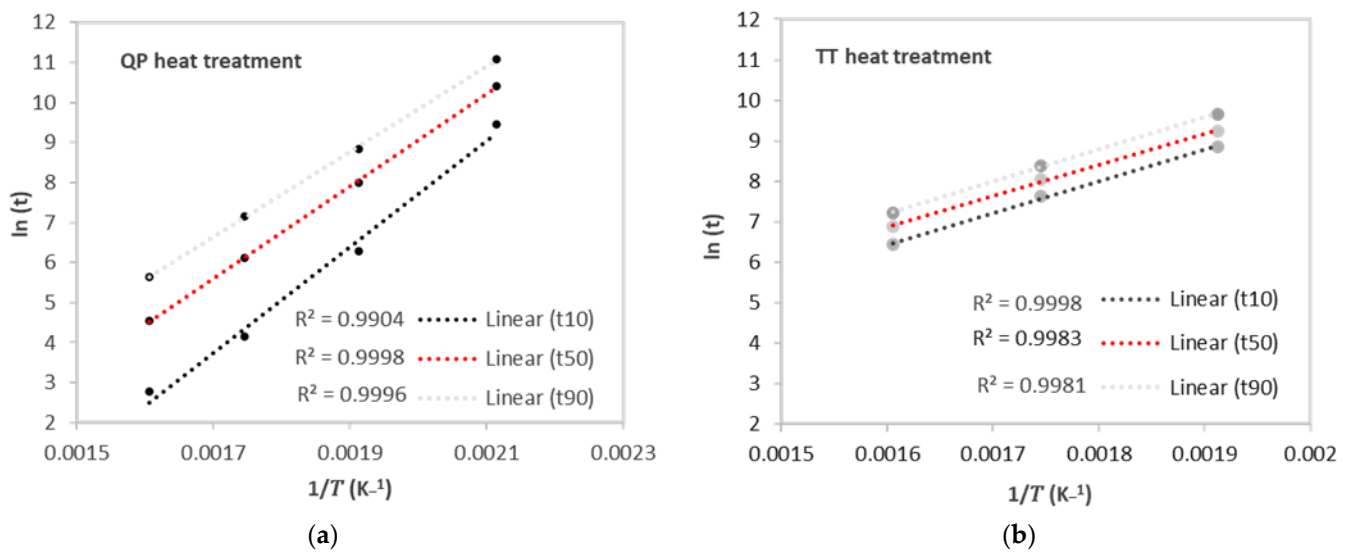


Figure 6. Arrhenius plot of $\ln(t_i)$ versus $1/T$ used to determine the activation energy: (a) QP; (b) TT.

The activation energy for isothermal transformation is in the range of 64 kJ/mol to 110 kJ/mol, which is less than that required for carbon diffusion in austenite (130 kJ/mol). This means that for the as-received high-carbon low-silicon steel, bainite growth is the dominant phenomenon as opposed to the competitive carbon partitioning. This conclusion is in agreement with the microstructural investigation where bainite growth was observed in the isothermal transformation temperature range of 200 to 350 °C instead of austenite stabilization by carbon partitioning.

4. Conclusions

A comparison was made between isothermal bainite formation (TT) in high-carbon steel containing 0.21 wt% silicon in the absence of pre-existing martensite, and bainite transformation in the presence of pre-existing martensite (QP).

The bainite starting and finishing times reduced significantly by having 20–30% pre-existing martensite in two-step heat treatments compared to isothermal transformation. Specifically, pre-existing martensite shortened the starting time to bainite formation in the temperature range of 250 to 350 °C by up to 70% at a temperature of 350 °C.

The hardness of complex microstructures consisting of pre-existing martensite, bainite, and retained austenite increased by 50 HV compared to isothermally produced bainite at partitioning temperatures of 250 and 300 °C, but there were no differences at 350 °C.

The kinetics of lower bainite formation was investigated by Avrami analysis. The experimentally determined n-index indicates that in the absence of pre-existing martensite, bainite nucleates at a constant rate, while in the presence of pre-existing martensite, bainite formation is controlled by nucleation and diffusion.

The apparent activation energy required to transform austenite to bainite was 65 KJ/mol, which is close to the activation energy for carbon diffusion in ferrite. The activation energy to form bainite increases in the presence of pre-existing martensite. In this instance, bainite start to form at the martensite/austenite interface. However, the activation energy in all of the heat treatments is less than the activation energy for carbon diffusion in austenite (130 kJ/mol). The implication is that in the high-carbon, low-silicon steel under investigation, bainite forms by an advancing austenite/bainite interface instead of by carbon partitioning and austenite stabilization.

Author Contributions: Z.B. designed and performed the experiments and data analysis. S.C.M. conducted the microscopy analysis. A.V.P. helped to design and analyze the magnetic measurements. R.D. supervised the study, suggested experimental approaches, helped to analyze experimental data, and revised the manuscript. F.P. and M.D.T. gave suggestions to revise the manuscript. Z.B. wrote the manuscript. All authors have read and agreed to the published version of the manuscript.

Funding: This research was supported under the Australian Research Council’s Industrial Transformation Research Hub funding scheme (project IH130200025).

Data Availability Statement: The data that support the findings of this study are available from the corresponding author upon reasonable request.

Acknowledgments: We gratefully acknowledge the access to the experimental facilities provided by The University of Wollongong and UNSW for the permission to publish the research outcomes.

Conflicts of Interest: The authors declare no conflict of interest.

References

1. Speer, J.G.; Rizzo, F.; Krauss, G.; Streicher, A.M.; Matlock, D. Quenching and Partitioning: A Fundamentally New Process to Create High Strength TRIP Sheet Microstructures. In Proceedings of the Austenite Formation and Decomposition, Chicago, IL, USA, 1 November 2003.
2. Speer, J.G.; Assunção, F.C.R.; Matlock, D.K.; Edmonds, D.V. The “quenching and partitioning” process: Background and recent progress. *Mater. Res.* **2005**, *8*, 417–423. [[CrossRef](#)]
3. Edmonds, D.; He, K.; Miller, M.K.; Rizzo, F.; Clarke, A.; Matlock, D.K.; Speer, J.G. Microstructural Features of ‘Quenching and Partitioning’: A New Martensitic Steel Heat Treatment. *Mater. Sci. Forum* **2007**, *539–543*, 4819–4825. [[CrossRef](#)]
4. Edmonds, D.; He, K.; Rizzo, F.; De Cooman, B.; Matlock, D.; Speer, J. Quenching and partitioning martensite—A novel steel heat treatment. *Mater. Sci. Eng. A* **2006**, *438–440*, 25–34. [[CrossRef](#)]
5. Huyghe, P.; Malet, L.; Caruso, M.; Georges, C.; Godet, S. On the relationship between the multiphase microstructure and the mechanical properties of a 0.2C quenched and partitioned steel. *Mater. Sci. Eng. A* **2017**, *701*, 254–263. [[CrossRef](#)]
6. de Diego-Calderón, I.; Sabirov, I.; Molina-Aldareguia, J.; Föjer, C.; Thiessen, R.; Petrov, R. Microstructural design in quenched and partitioned (Q&P) steels to improve their fracture properties. *Mater. Sci. Eng. A* **2016**, *657*, 136–146. [[CrossRef](#)]
7. Yan, S.; Liu, X.; Liu, W.J.; Liang, T.; Zhang, B.; Liu, L.; Zhao, Y. Comparative study on microstructure and mechanical properties of a C-Mn-Si steel treated by quenching and partitioning (Q&P) processes after a full and intercritical austenitization. *Mater. Sci. Eng. A* **2017**, *684*, 261–269. [[CrossRef](#)]
8. He, S.; He, B.; Zhu, K.; Ding, R.; Chen, H.; Huang, M. Revealing the role of dislocations on the stability of retained austenite in a tempered bainite. *Scr. Mater.* **2019**, *168*, 23–27. [[CrossRef](#)]
9. Samanta, S.; Das, S.; Chakrabarti, D.; Samajdar, I.; Singh, S.B.; Haldar, A. Development of Multiphase Microstructure with Bainite, Martensite, and Retained Austenite in a Co-Containing Steel Through Quenching and Partitioning (Q&P) Treatment. *Met. Mater. Trans. A* **2013**, *44*, 5653–5664. [[CrossRef](#)]
10. Garcia-Mateo, C.; Caballero, F.G.; Sourmail, T.; Cornide, J.; Smanio, V.; Elvira, R. Composition design of nanocrystalline bainitic steels by diffusionless solid reaction. *Met. Mater. Int.* **2014**, *20*, 405–415. [[CrossRef](#)]
11. Sourmail, T.; Caballero, F.; Garcia-Mateo, C.; Smanio, V.; Ziegler, C.; Kuntz, M.; Elvira, R.; Leiro, A.; Vuorinen, E.; Teeri, T. Evaluation of potential of high Si high C steel nanostructured bainite for wear and fatigue applications. *Mater. Sci. Technol.* **2013**, *29*, 1166–1173. [[CrossRef](#)]
12. Sourmail, T.; Caballero, F.; Moudian, F.; De Castro, D.; Benito, M. High hardness and retained austenite stability in Si-bearing hypereutectoid steel through new heat treatment design principles. *Mater. Des.* **2018**, *142*, 279–287. [[CrossRef](#)]
13. Quidort, D.; Bréchet, Y. The role of carbon on the kinetics of bainite transformation in steels. *Scr. Mater.* **2002**, *47*, 151–156. [[CrossRef](#)]
14. Nayak, S.; Anumolu, R.; Misra, R.; Kim, K.; Lee, D. Microstructure–hardness relationship in quenched and partitioned medium-carbon and high-carbon steels containing silicon. *Mater. Sci. Eng. A* **2008**, *498*, 442–456. [[CrossRef](#)]
15. Garcia-Mateo, C.; Caballero, F.G.; Bhadeshia, H.K.D.H. Acceleration of Low-temperature Bainite. *ISIJ Int.* **2003**, *43*, 1821–1825. [[CrossRef](#)]
16. Goulas, C.; Mecozzi, M.G.; Sietsma, J. Bainite Formation in Medium-Carbon Low-Silicon Spring Steels Accounting for Chemical Segregation. *Met. Mater. Trans. A* **2016**, *47*, 3077–3087. [[CrossRef](#)]
17. Dong, J.; Vethers, H.; Hoffmann, F.; Zoch, H.W.; Beswick, J.; Dean, S.W. Microstructure and Fatigue Strength of the Bearing Steel 52100 after Shortened Bainitic Treatment. *J. ASTM Int.* **2010**, *7*, 17–31. [[CrossRef](#)]
18. Sourmail, T. Bainite and Superbainite in Long Products and Forged Applications. *HTM J. Heat Treat. Mater.* **2017**, *72*, 371–378. [[CrossRef](#)]
19. Navarro-López, A.; Sietsma, J.; Santofimia, M.J. Effect of Prior Athermal Martensite on the Isothermal Transformation Kinetics Below M_s in a Low-C High-Si Steel. *Met. Mater. Trans. A* **2015**, *47*, 1028–1039. [[CrossRef](#)]

20. Navarro-López, A.; Hidalgo, J.; Sietsma, J.; Santofimia, M. Influence of the prior athermal martensite on the mechanical response of advanced bainitic steel. *Mater. Sci. Eng. A* **2018**, *735*, 343–353. [[CrossRef](#)]
21. Kawata, H.; Hayashi, K.; Sugiura, N.; Yoshinaga, N.; Takahashi, M. Effect of Martensite in Initial Structure on Bainite Transformation. *Mater. Sci. Forum* **2010**, *638–642*, 3307–3312. [[CrossRef](#)]
22. Santofimia, M.J.; Van Bohemen, S.M.C.; Sietsma, J. Combining bainite and martensite in steel microstructures for light weight applications. *J. S. Afr. Inst. Min. Metall.* **2013**, *113*, 143–148.
23. Ravi, A.M.; Sietsma, J.; Santofimia, M.J. Exploring bainite formation kinetics distinguishing grain-boundary and autocatalytic nucleation in high and low-Si steels. *Acta Mater.* **2016**, *105*, 155–164. [[CrossRef](#)]
24. Smanio, V.; Sourmail, T. Effect of Partial Martensite Transformation on Bainite Reaction Kinetics in Different 1% C Steels. *Solid State Phenom.* **2011**, *172–174*, 821–826. [[CrossRef](#)]
25. Veters, H.; Dong, J.; Bomas, H.; Hoffmann, F.; Zoch, H.-W. Microstructure and fatigue strength of the roller-bearing steel 100Cr6 (SAE 52100) after two-step bainitisation and combined bainitic–martensitic heat treatment. *Int. J. Mater. Res.* **2006**, *97*, 1432–1440. [[CrossRef](#)]
26. Toji, Y.; Matsuda, H.; Raabe, D. Effect of Si on the acceleration of bainite transformation by pre-existing martensite. *Acta Mater.* **2016**, *116*, 250–262. [[CrossRef](#)]
27. Hu, F.; Wu, K. Nanostructured high-carbon dual-phase steels. *Scr. Mater.* **2011**, *65*, 351–354. [[CrossRef](#)]
28. Ravi, A.M.; Sietsma, J.; Santofimia, M.J. Bainite formation kinetics in steels and the dynamic nature of the autocatalytic nucleation process. *Scr. Mater.* **2017**, *140*, 82–86. [[CrossRef](#)]
29. Shah, M.; Das, S.K.; Pastor, A. Phenomenological kinetic model of the nano-bainitic steels to characterize the dynamics of the autocatalytic nucleation process. *SN Appl. Sci.* **2020**, *2*, 635. [[CrossRef](#)]
30. Guimarães, J.R.C.; Rios, P.R.; Alves, A.L.M. An Alternative to Avrami Equation. *Mater. Res.* **2019**, *22*. [[CrossRef](#)]
31. Li, H.; Gai, K.; He, L.; Zhang, C.; Cui, H.; Li, M. Non-isothermal phase-transformation kinetics model for evaluating the austenization of 55CrMo steel based on Johnson–Mehl–Avrami equation. *Mater. Des.* **2016**, *92*, 731–741. [[CrossRef](#)]
32. Quidort, D.; Bréchet, Y.J.M. A Model of Isothermal and Non Isothermal Transformation Kinetics of Bainite in 0.5% C Steels. *ISIJ Int.* **2002**, *42*, 1010–1017. [[CrossRef](#)]
33. Kuklina, A.A.; Maisuradze, M.V.; Yudin, Y.V. Analytical Description of the Bainite Transformation Kinetics in Steels 300M and D6AC. *Mater. Sci. Forum* **2017**, *907*, 31–37. [[CrossRef](#)]
34. Ruitenbergh, G.; Woltd, E.; Petford-Long, A. Comparing the Johnson–Mehl–Avrami–Kolmogorov equations for isothermal and linear heating conditions. *Thermochim. Acta* **2001**, *378*, 97–105. [[CrossRef](#)]
35. Van Bohemen, S.M.C.; Sietsma, J. Kinetics of martensite formation in plain carbon steels: Critical assessment of possible influence of austenite grain boundaries and autocatalysis. *Mater. Sci. Technol.* **2014**, *30*, 1024–1033. [[CrossRef](#)]
36. Zhu, J.G. Bainite Transformation Kinetics-Microstructure Characterization of Austempered 4140/4150 Steel. Ph.D. Thesis, Oakland University, Rochester, MI, USA, 2019.
37. Babasafari, Z.; Pan, A.V.; Pahlevani, F.; Hossain, R.; Sahajwalla, V.; du Toit, M.; Dippenaar, R. Effects of austenizing temperature, cooling rate and isothermal temperature on overall phase transformation characteristics in high carbon steel. *J. Mater. Res. Technol.* **2020**, *9*, 15286–15297. [[CrossRef](#)]
38. Babasafari, Z.; Pan, A.V.; Pahlevani, F.; Kong, C.; Du Toit, M.; Dippenaar, R. Effect of Microstructural Features on Magnetic Properties of High-Carbon Steel. *Met. Mater. Trans. A* **2021**, *52*, 5107–5122. [[CrossRef](#)]
39. Babasafari, Z.; Pan, A.V.; Pahlevani, F.; Kong, C.; Sahajwalla, V.; du Toit, M.; Dippenaar, R. Effect of silicon and partitioning temperature on the microstructure and mechanical properties of high-carbon steel in a quenching and partitioning heat treatment. *J. Mater. Sci.* **2021**, *56*, 15423–15440. [[CrossRef](#)]
40. Damon, J.; Mühl, F.; Dietrich, S.; Schulze, V. A Comparative Study of Kinetic Models Regarding Bainitic Transformation Behavior in Carburized Case Hardening Steel 20MnCr5. *Met. Mater. Trans. A* **2018**, *50*, 104–117. [[CrossRef](#)]
41. Zhu, J.G.; Sun, X.; Barber, G.C.; Han, X.; Qin, H. Bainite Transformation-Kinetics-Microstructure Characterization of Austempered 4140 Steel. *Metals* **2020**, *10*, 236. [[CrossRef](#)]
42. van Bohemen, S. Autocatalytic nature of the bainitic transformation in steels: A new hypothesis. *Philos. Mag.* **2013**, *93*, 388–408. [[CrossRef](#)]
43. Kang, M.; Zhang, M.-X.; Liu, F.; Zhu, M. Kinetics and Morphology of Isothermal Transformations at Intermediate Temperature in 15CrMnMoV Steel. *Mater. Trans.* **2009**, *50*, 123–129. [[CrossRef](#)]
44. Askeland, D.R. Atom Movement in Materials. In *The Science and Engineering of Materials*; Springer: Boston, MA, USA, 1996; Chapter 5, pp. 111–137.